JOURNAL OF PROPULSION AND POWER
Vol. 14, No. 6, November–December 1998

Numerical Simulation of Hypersonic Shock-Induced Combustion Ramjets

R. Dudebout,* J. P. Sislian,† and R. Oppitz‡
University of Toronto, Downsview, Ontario M3H 5T6, Canada

Hypersonic air-breathing propulsion utilizing shock-induced combustion ramjets is investigated. Two-dimensional geometries are simulated with planar and axisymmetric configurations, as well as external and mixed-compression configurations. The lower–upper Symmetric Gauss–Seidel scheme combined with a symmetric shock-capturing total variation diminishing scheme are used to solve the Euler equations, with nonequilibrium chemical reactions. The finite rate chemistry model includes 13 species (H_2, O_2, H, O, OH, H_2O, HO_2, H_2O_2, N, NO, HNO, N_2, and NO_2) and 33 reactions. The numerical method has been verified by comparison with H_2/air induction delay times, analytical solutions to wedge problems, and exothermic blunt body flows. Results obtained with an inviscid, chemically nonequilibrium numerical approach and with realistic geometries demonstrate that shock-induced combustion can be used as a viable means of hypersonic propulsion. As part of the combustor design, it has also been numerically demonstrated that a minimum-entropy, or Chapman–Jouguet condition exists for oblique-detonation waves generated by wedges in nonequilibrium chemically reacting H_2/air flowfields.

Nomenclature

E = total energy, J
$\boldsymbol{F}$ = flux vector in ξ direction
$\boldsymbol{G}$ = flux vector in η direction
H = Jacobian of source terms $\sigma\boldsymbol{S} - \boldsymbol{W}$
H_k = specific enthalpy of species k, J/kg
I_{sp} = fuel specific impulse, s
J = metric Jacobian
M = Mach number
$\mathcal{M}_k$ = molecular weight of species k
P = pressure, Pa
$\boldsymbol{Q}$ = vector of conservative variables
q_{dyn} = dynamic pressure, Pa or lb/ft^2
$\mathcal{R}$ = universal gas constant, J/kg K
$\boldsymbol{S}$ = vector of axisymmetric source terms
T = temperature, K
t = time, s
U = contravariant velocity in the ξ direction
u = longitudinal velocity component, m/s
V = contravariant velocity in the η direction
v = transverse velocity component, m/s
$\boldsymbol{W}$ = vector of species production source terms
x = longitudinal coordinate of physical reference frame, m
y = transverse coordinate of physical reference frame, m
β = oblique shock wave angle
γ = specific heat ratio
δ = semiangle of cone or wedge
η = transverse coordinate of computational reference frame
θ = flow angle
ξ = longitudinal coordinate of computational reference frame
ρ = density, kg/m^3
ρ_k = density of species k, kg/m^3
ν = 0 (planar) or 1 (axisymmetric)
φ = equivalence ratio = 1

Subscripts
k = species number
w = wall
∞ = freestream conditions

Presented as Paper 94-3098 at the AIAA/ASME/SAE/ASEE 30th Joint Propulsion Conference, Indianapolis, IN, June 27–29, 1994; received March 28, 1997; revision received Feb. 20, 1998; accepted for publication April 10, 1998.

*Research Associate, Institute for Aerospace Studies; currently Research Engineer, Pratt and Whitney Canada, United Technologies Corporation, Combustion Section, Mississauga, Ontario L5T 1J3, Canada.

†Professor, Institute for Aerospace Studies. E-mail: sislian@moebius.utias.utoronto.ca. Associate Fellow AIAA.

‡Graduate Student, Institute for Aerospace Studies; currently Management Consultant, PricewaterhouseCoopers, Information Technology Services, Toronto, Ontario, Canada.

Introduction

IT has long been established that the engine cycle of choice for hypersonic air-breathing propulsion is the supersonic-combustion ramjet or scramjet. In this type of engine, to avoid very high temperatures and, consequently, high levels of dissociation of air and combustion products as well as excessive structural heat loads, the oncoming air captured and compressed by the inlet of the engine remains supersonic up to the entry of the combustor. Therefore, the combustion of the injected fuel takes place at supersonic speeds and can be organized in a number of ways. The more conventional way is to mix and burn the fuel simultaneously and this diffusive burning mode has been the main focus of present-day high-speed propulsion research. For the lower flight Mach number range (6–12) efficient fuel/air mixing in a supersonic flow can be achieved by transverse fuel injection, as well as by instream injection. However, as the flight Mach number increases, the losses incurred by this mode of mixing increase and streamwise (parallel) injection is increasingly employed to alleviate these losses and also to recover the thrust from the fuel injection process that becomes significant at hypersonic velocities.[1] It is well known that compressibility effects in high-Mach-number flows decrease the growth rate of mixing layers, thus significantly reducing the mixing and, consequently, the combustion efficiencies. Therefore, to achieve the desired levels of diffusive burning efficiency, the combustor must be fairly long. Because the highest pressures and temperatures in the scramjet occur in the combustor, its weight and drag will increase ac-

cordingly and will form a significant fraction of the empty weight of the vehicle. Recently, a variety of mixing-enhancement techniques have been proposed to alleviate this problem.[2,3]

One way out of this situation is to decouple the fuel/air mixing and combustion processes. In this scramjet concept, fuel/air mixing is organized in the vehicle forebody flow, which also serves as the inlet of the engine, taking care to avoid or delay ignition of the fuel/air mixture. Combustion in the more or less homogeneous fuel/air mixture is then achieved by a conveniently located shock wave that raises the temperature and pressure to its ignition point. If ignition occurs far enough downstream that the ensuing combustion process does not influence the preceding shock, the combustion is said to be shock induced. This is the shock-induced combustion ramjet (shcramjet[4]). For extremely fast reactions, ignition occurs close to the preceding shock wave and the combustion process couples with the shock wave and forms a detonation wave. Therefore, the detonation wave ramjet is a particular case of the shcramjet.

It is clear that in the shcramjet concept, the previously mentioned technically challenging task of reducing the scramjet combustor length at very high flight Mach numbers has been replaced by an equally formidable task of homogeneously mixing the streamwise injected fuel with the hypervelocity forebody/inlet shock-layer flow prior to combustion. However, in this case the forebody/inlet mixing problem may be mitigated by the relatively long residence time the fuel will have in the propulsive airstream contained by the long and slender forebody inlet of the vehicle. During the fuel/air mixing process, ignition of the fuel at the point of injection, in the inlet flow, and in the wall boundary layers must be minimized, and accurate estimates of losses accruing from all of these processes must be established. Other practical issues that must be resolved to achieve satisfactory operation of shcramjets are experimental and theoretical evidence of the stability of detonation waves, and conditions under which such waves are possible, at all required combustor inlet values of velocity, pressure, temperature and fuel/air ratio; control of boundary-layer separation caused by shock-induced combustion or detonation wave; and realistic estimates of propulsive characteristics of such ramjets. It is clear that a substantial amount of research and development is needed for the practical implementation of shcramjets.

If implemented, the advantages of the shcramjet over the scramjet are many. The shock component of the detonation or shock-induced combustion process provides the additional large compression and the corresponding high temperatures required for rapid combustion. Consequently, the compression process in the inlet of the shcramjet is less than that for the scramjet, and, therefore, the losses involved in flow deceleration in the inlet are reduced. Also, with the proper choice of fluid dynamic and geometric parameters of the shcramjet configuration for given flight conditions, the shock-induced combustion process will be very rapid and will occur over a very short distance from the shock, resulting in a short combustor length, less combustor cooling load, and an overall shorter and lightweight engine system than for the scramjet. Considering that for acceleration missions, such as the single stage to orbit vehicle, the engine weight is a strong concern, these advantages are not insignificant.

However, despite these advantages, the full potential of the shcramjet has not yet been explored in a systematic manner. This mode of heat addition to a supersonic flow was advanced in 1946 by Roy.[5] Earliest work in this area was that of Dunlap et al.[6] and Sargeant and Gross.[7] They presented engine performance characteristics (specific thrust, specific fuel consumption) in the flight Mach number range $3 < M_\infty < 10$, based on a simplified one-dimensional analysis. Townend[8] studied a more elaborate hypersonic detonation wave ramjet configuration consisting of multishock diffusers, optimized by the Oswatitch criterion, i.e., having shocks of equal strength, matched to overdriven or Chapman–Jouguet detonation waves, normal or oblique, in such a way as to minimize the net total pressure loss in the inlet and heat addition processes. He derived an analytical expression for this optimum condition. He concluded that heat addition by Chapman–Jouguet detonation is competitive with heat addition at constant pressure. He emphasized the "need for research on oblique rather than normal detonation and conical rather than planar waves."

Morrison[9,10] published two reports on oblique detonation wave ramjets, in which he studied in detail multishock external and mixed compression diffusers, fuel injection losses, combustion chamber configurations, and the effects of chemistry on oblique detonation wave ramjets and of real gas effects on nozzle expansion. Estimates of the propulsive performance of external and mixed compression ramjets were also reported based on simplified one-dimensional analysis. He concluded that "the oblique detonation wave ramjet offers a great potential as an airbreathing propulsor to extend the useful range of ramjet flight Mach numbers from 6 to 16 and above. Specific impulses and thrust coefficients that would be obtainable in the above flight range would exceed 70 percent of ideal." Detonation wave ramjets were also investigated by Billig[11,12] within the context of a wider study of external burning in supersonic streams. The concept of heat addition to a supersonic flow by shock-induced combustion has been actively developed in the former USSR.[13,14]

A revival of interest has occurred lately in detonation wave ramjet propulsion for hypersonic flight. The oblique detonation wave engine in combination with a dual-fuel, dual-expander rocket engine has been proposed as a propulsion device for a single stage to orbit vehicle.[15] The analysis performed by Morrison[10] has been taken a step further by assuming more realistic working gas properties and considering a more elaborate detonation wave model.[16] The estimated performance parameters (fuel specific impulse, thrust per unit inlet area, etc.) are essentially based on a one-dimensional cycle-type analysis rather than on a specific vehicle geometry. A one-dimensional cycle analysis approach to oblique detonation wave engine performance based on a real gas model with equilibrium H_2/air and CH_4/air chemistry has also been presented.[17] Computational fluid dynamic methods together with a Chapman–Jouguet detonation wave model or a shock-induced finite rate hydrogen/air combustion process were used[4,18–25] to determine the entire flowfield of a class of hypersonic planar and axisymmetric, external, and mixed compression shcramjet models and assess their aerodynamic and propulsive performance characteristics. Three-dimensional waverider configurations derived from these studies were also investigated. An analysis of the performance of a conceptual transatmospheric vehicle powered by an oblique detonation wave engine was undertaken by Menees et al.[26] Similar investigations were also performed in the related field of detonation wave-driven projectiles in tubes, the so-called ram accelerator, by a number of researchers.[27–31]

In the present paper the aeropropulsive performance parameters of the shcramjet are derived from the numerical simulation of the entire hypersonic flowfield around a specific planar or axisymmetric shock-induced combustion ramjet model. Therefore, the presented inviscid flowfield and propulsive characteristics of the shcramjet may be viewed as a first-look approach at investigating the viability of shcramjets. The introduction of the geometry of the engine in the cycle analysis was deemed necessary for further detailed exploration such as the following real vehicle issues: 1) off-design conditions when, for example, the vehicle is flying at flight Mach numbers for which it was not designed, or the effect of nonuniform (as opposed to uniform, homogeneous) fuel/air distribution in the propulsive streamtube on the performance of the engine; 2) viscous-related effects such as boundary-layer thicknesses in various components of the shcramjet, frictional drag of the model vehicle, shock, and detonation wave–boundary-layer in-

teraction; and 3) fuel/air mixing in a realistic geometry and flow situation and control of preignition.

Governing Equations and Computational Technique

The shcramjet flowfield is described by the Euler equations for a reacting gas and a planar or axisymmetric flow configuration. In a curvilinear coordinate system, they can be written in the following form:

$$\frac{\partial \boldsymbol{Q}}{\partial t} + \frac{\partial \boldsymbol{F}}{\partial \xi} + \frac{\partial \boldsymbol{G}}{\partial \eta} = \boldsymbol{S} \tag{1}$$

where

$$\boldsymbol{Q} = J^{-1} \begin{Bmatrix} \rho_1 \\ \vdots \\ \rho_{ns} \\ \rho u \\ \rho v \\ E \end{Bmatrix}$$

$$\boldsymbol{F} = J^{-1} \begin{Bmatrix} \rho_1 U \\ \vdots \\ \rho_{ns} U \\ \rho u U + \xi_x P \\ \rho v U + \xi_y P \\ U(E + P) \end{Bmatrix}, \qquad \boldsymbol{G} = J^{-1} \begin{Bmatrix} \rho_1 V \\ \vdots \\ \rho_{ns} V \\ \rho u V + \eta_x P \\ \rho v V + \eta_y P \\ V(E + P) \end{Bmatrix}$$

$$\boldsymbol{S} = J^{-1} \begin{Bmatrix} w_1 \\ \vdots \\ w_{ns} \\ 0 \\ 0 \\ 0 \end{Bmatrix} - \frac{\nu J^{-1}}{y} \begin{Bmatrix} \rho_1 v \\ \vdots \\ \rho_{ns} v \\ \rho u v \\ \rho v^2 \\ v(E + P) \end{Bmatrix}$$

The contravariant velocities U and V, and the Jacobian J are defined by

$$U = \xi_x u + \xi_y v$$

$$V = \eta_x u + \eta_y v$$

$$J^{-1} = x_\xi y_\eta - x_\eta y_\xi$$

In the preceding expressions, $\nu = 0$ for planar and $\nu = 1$ for axisymmetric flows; n_s is the number of species; ρ_k is the density of the species k; w_k is the production term resulting from chemical reactions for the species k; u and v are the velocity components in the x and y directions, respectively; and E is the internal energy. Temperature is implicitly determined from the definition of total energy

$$\sum_{k=1}^{ns} \frac{\rho_k}{\rho} H_k - \sum_{k=1}^{ns} \frac{\rho_k}{\rho} \frac{\mathcal{R}T}{\mathcal{M}_k} = \frac{E}{\rho} - \frac{1}{2}(u^2 + v^2)$$

P is then determined from the equation of state for a mixture of thermally perfect gases,

$$P = \sum_{k=1}^{ns} \frac{\rho_k}{\mathcal{M}_k} \mathcal{R}T$$

where H_k is the enthalpy of species k (including the heat of formation at 0 K). The finite-rate combustion process of the hydrogen/air mixture is described by 33 reactions between 13 species (H_2, O_2, H, O, OH, H_2O, HO_2, H_2O_2, N, NO, HNO, N_2, and NO_2). The rate coefficients used for the forward reactions are those given by Jachimowsky.[32] The rate coefficients for the reverse reactions were calculated from the forward-rate coefficients and the appropriate equilibrium constants. All thermochemical data for the hydrogen, oxygen, and nitrogen species were calculated with NASA polynomials of the JANAF (1971) tables.

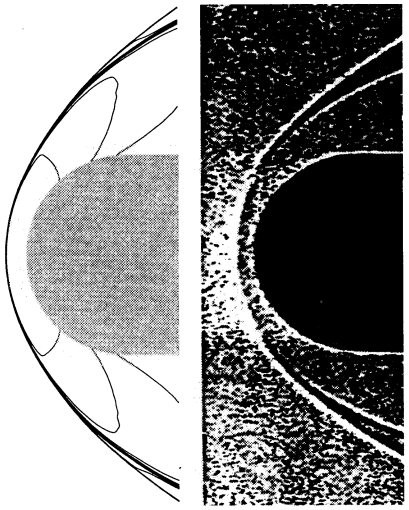

numerical results Lehr's results

Fig. 1 Comparison of numerical solution on a 180 × 270 evenly spaced mesh and experimental results.

The numerical method employed is a fully implicit, fully coupled, Newton-iteration, total variation diminishing (TVD) scheme for solving nonequilibrium, chemically reacting flows at steady state. It combines the lower–upper symmetric Gauss–Seidel (LUSGS) method developed by Jameson and Yoon[33,34] and a TVD scheme developed by Yee.[35]

Code Validation

The computational technique has been validated by comparisons of the predicted 1) ignition delay times with Jachimowski,[25,32] 2) planar and conical shock wave angles with analytical solutions,[25] and 3) exothermic blunt body flows with Lehr's experimental results.[36] In the latter case, a 180 × 270 grid was used to find the numerical solution.[37] The results are presented in Fig. 1. The numerical results clearly show that the bow shock and flame front split, although the radial distance of the shock at the exit plane is still about 13% overpredicted compared to Lehr's results. Drabczuk et al.[38] demonstrate the need for adequate spatial resolution of the reaction induction zone. They very accurately predict Lehr's results by using adaptive gridding. Without adaptive gridding, excessive mesh refinements are required.

A grid convergence study was undertaken on a double-wedge, planar, 15-m-long inlet for a Mach 14 shcramjet, at q = 1400 psf (67,032 Pa). To compare with the analytical solution, calorically perfect air (specific heat ratio of 1.4) was used. Figure 2a presents the domain for a 48 × 24 grid. This flowfield was solved such that the L2 norm of density change between successive time steps was less than 10^{-6} for each case. The predicted lift is compared to the analytical solution. Figure 2b demonstrates the reduction of error in predicted lift as the total number of nodes is successively refined. Figure 2c depicts the temperature profiles across an oblique detonation wave for different grid systems. The numerical results presented in the following sections use 9100 nodes (130 × 70) in the inlet section, which guarantees <1% error in predicted lift and drag.

Shcramjet Model

Inlet

Two types of multishock external (Fig. 3, configuration I) and mixed (configuration II) compression inlets were consid-

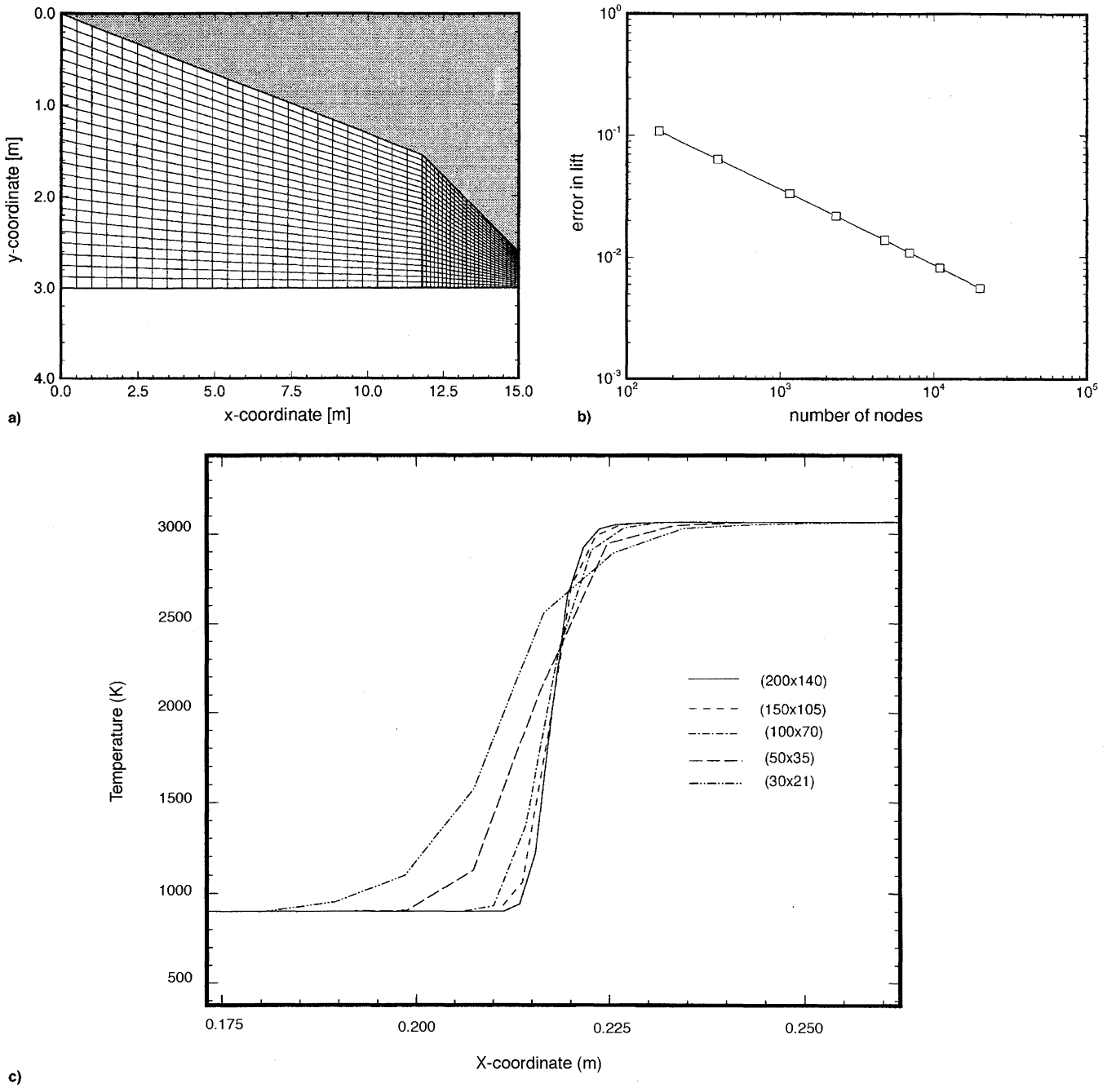

Fig. 2 Grid convergence case study: a) 48 × 24 computational grid for M_∞ = 14, q_{dyn} = 1400 psf (67,032 Pa) double-wedge case; b) error in predicted lift vs number of nodes for M_∞ = 14, q_{dyn} = 1400 psf (67,032 Pa) double-wedge case; and c) temperature profiles across an oblique H_2/air detonation wave for M_∞ = 7 and δ_{wedge} = 15 deg, for different grid systems.

ered. Configuration I employs two equal-strength shocks (to minimize entropy increase), whereas a three-equal-strength shock system is assumed for configuration II. At the design point considered in the present paper, the two shocks in configuration I are assumed to intersect at the cowl tip C, whereas for configuration II, the cowl tip B will always be situated on the bow shock AB. It is also assumed that fuel (H_2) is injected in the forebody/inlet flow parallel to the oncoming airflow and that a homogeneous mixture results at the combustor entrance section (DC in configuration I and DD′ in configuration II). To simulate this, the portion of the oncoming flow above the cowl tip (labeled "inner flow" in Fig. 3) is assumed to be a homogeneous hydrogen/air mixture at an equivalence ratio of 1. The portion of the flow below the leading edge of the cowl (labeled "outer flow" in Fig. 3) is composed of air only. It is assumed that the temperature, pressure, and velocity are identical for the inner and outer flows. However, because of the differences in composition of the inner and outer flows, the density and Mach number differ. The temperature of the inner flow at the end of the compression process must be sufficiently low to guarantee that the ignition delay is long enough to prevent burning in the inlet. Hence, the maximum compression temperature at the combustor inlet (DC and DD′) is set, arbitrarily, at 900 K, ensuring that no premature ignition occurs. The inlet length (axial distances AC′ or AB′, Fig. 3) is fixed at 15 m. These requirements uniquely determine the planar or axisymmetric inlet surface geometry. The inlet flowfield is solved iteratively using the nonreacting version of the developed Euler code. The dotted lines CD or DD′ (Fig. 3) represent the exit plane of the inlet and the grid points, where the flow variables are extracted and used as inflow to the combustion system.

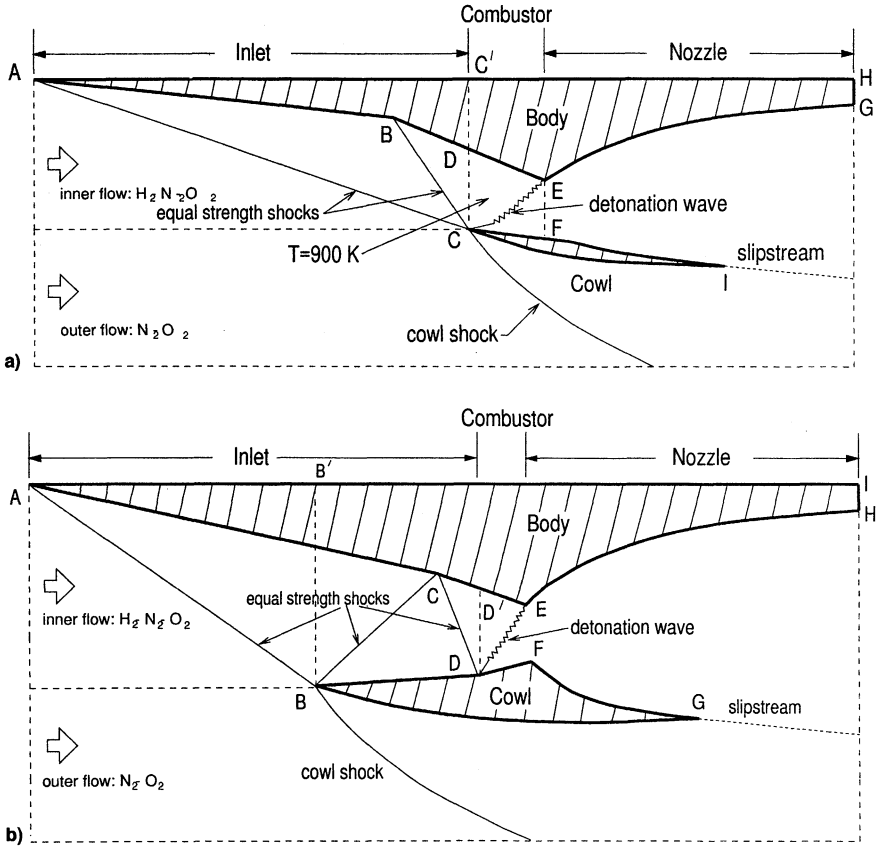

Fig. 3 Shcramjet model (axisymmetric or planar). Configurations a) I and b) II.

Combustor

The oblique detonation wave is generated by the cowl surface CF or DF (see Fig. 3). Referring to Fig. 4, the combustor design proceeds by varying the cowl angle δ measured from the axis and solving the Euler equations with the LUSGS scheme for the resulting flowfield. Figure 5 shows the temperature contours for an oblique detonation wave (ODW) on a wedge of angle $\delta_w = 5.0$ deg, $M_\infty = 7.0$, $T_\infty = 900$ K, and $P_\infty = 23{,}000$ Pa, and represents the flow structure typical of a nonequilibrium ODW. After a certain ignition delay distance, where the reaction radicals increase in concentration by an order of magnitude, but no heat is yet released (see Jachimowsky[32] for greater detail), ignition occurs on the wedge surface. The ensuing shock-induced flamefront intersects the wedge shock and a combined shock/flame-front (detonation) wave emerges. Thus, the nonequilibrium flow introduces a length scale (the ignition delay distance or the induction distance), which is sensitive to both pressure and temperature and, hence, to wedge angle δ_w. The flow over wedge angles between $\delta = 5$ and 30 deg (in increments of 2.5 deg) were determined. The inflow at the left boundary is obtained from the distribution of flow variables along line CD (or DD′) (Fig. 3), from the inlet flowfield. The body surface in the combustor section, line DE or D′E, can be determined by tracking the streamline starting at the coordinates of point D or D′ (inlet exit point on the body surface) through the combustor section until the detonation wave is intercepted. To determine the Chapman–Jouguet angle, and, therefore, the minimum entropy, the deflection angle is decreased until the detonation wave ceases to decrease. The net deflection and detonation wave angles are plotted in Fig. 6 for the planar case, for the range of inner flow Mach numbers of interest. It can be surmised that for higher Mach numbers the flow is deflected to a lesser degree and the detonation wave is, therefore, weaker. Generally, the weaker the detonation wave, the longer the ignition delay; hence, at the Chapman–Jouguet point, the ignition delay

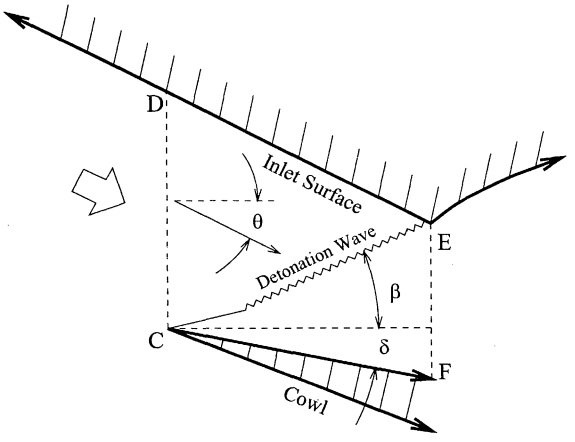

Fig. 4 Combustor design.

becomes exceedingly long for the higher Mach numbers (on the order of several meters). Noting that the entropy curve is rather shallow near the Chapman–Jouguet point, the 3-deg overdriven case was chosen for each combustor cowl angle, i.e., $\delta_{\text{combustor}} = \delta_{CJ} - 3$ deg, for all Mach numbers, thereby considerably shortening the ignition delay distance and, accordingly, the combustor, with no penalty in entropy rise. It can also be seen why the inlet length was chosen to be 15 m. For this inlet length and geometrically scaled intake area at the combustor, a shorter inlet length would lead to a combustion process consisting of shock-induced combustion, not detonation wave. Finally, the flow variables along the line EF in Fig. 4 are extracted to serve as inflow to the expansion system.

Nozzle

For purposes of determining the nozzle surfaces (walls), the flow in the nozzle is assumed to be chemically frozen and the

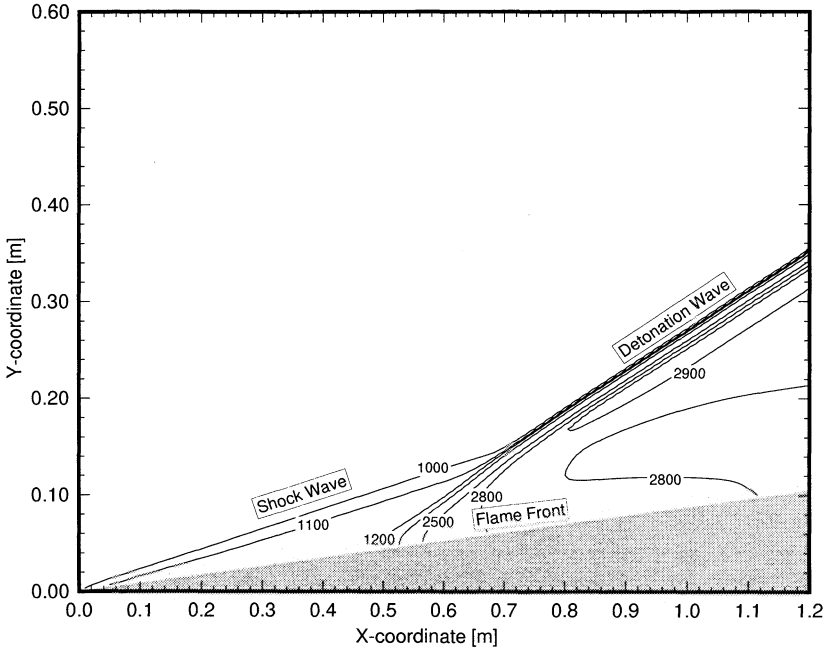

Fig. 5 Temperature contours of the shock-induced combustion/detonation flowfield generated by a wedge of δ_w = 5 deg for φ = 1, P_∞ = 23,000 Pa, T_∞ = 900 K, and M_∞ = 7.

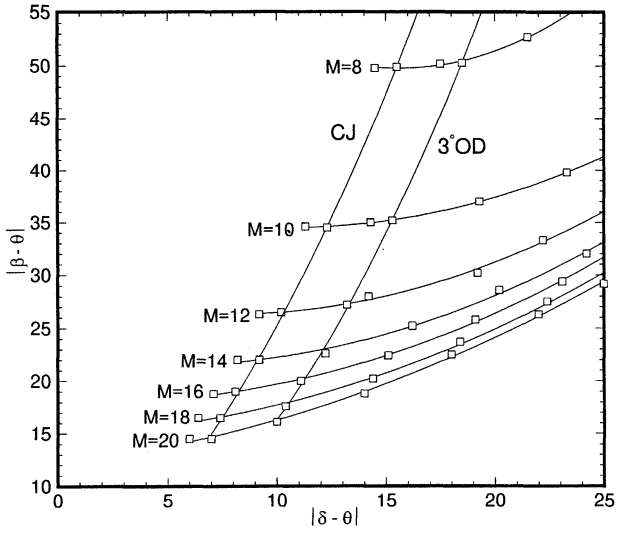

Fig. 6 Detonation wave angle vs deflection angle for planar shcramjets, 8 ≤ M_{inner} ≤ 20 and locus of Chapman–Jouguet and 3-deg overdriven angles.

method of characteristics used to build the central body and cowl inner surfaces by specifying a uniform flow in the axial direction at the exit plane of the nozzle. The exit pressure is iteratively determined to expand the nozzle flow to the axis of the vehicle. The initial values of the flow variables are extracted from the combustor exit section (line EF, Fig. 4) and averaged. Furthermore, average specific heats, total pressure, and temperature are calculated along the distribution, which is kept constant throughout the method of characteristics' calculations. The false-wall technique is used for configuration I, whereas a dual-wall technique[39–42] was found to be appropriate for configuration II (the false-wall technique would produce negative thrust for this configuration). Because both the body and cowl inner nozzle walls obtained were exceedingly long, they were cut off to provide 95% of their maximum thrust to reduce the frictional drag.

The outer (bottom) surface of the cowl is designed by prescribing a polynomial, matching the coordinates of the cowl tip and trailing edge of the inner surface. At the leading edge the cowl inclusion angle is prescribed to be 5 deg, and at the trailing edge it is set to be zero (parallel to the flow). Thus, the integrated shcramjet model is obtained by assembling all surfaces generated for each component and the entire shcramjet flowfield, from tip to tail, is determined by using the LUSGS method for the Euler equations for nonequilibrium reacting flow of H_2/air mixtures described previously.

At the trailing edge of the cowl (point I or G, Fig. 3), a contact surface is formed between the inner (propulsive stream tube) and outer (freestream deflected by the cowl shock) flows. It is important to approximately match the pressure across this interface, as the creation of a shock into the propulsive streamtube (as would occur if the pressure is less in the propulsive stream tube than in the outer flow) would adversely affect the shcramjet performance.

Shcramjet Flowfield Analysis

The Mach 14 planar external compression shcramjet, for a flight dynamic pressure of q = 1400 psf (67,032 Pa) and equivalence ratio φ = 1, will serve to illustrate particular features of the shcramjet flowfield. Of interest are the variations of flow parameters at lateral sections: 2, combustor exit plane; 3, cowl trailing-edge plane; and 4, the shcramjet exit plane (Fig. 7). Figure 7 shows the pressure distributions at lateral sections 2, 3, and 4. At the cowl trailing-edge plane, the pressure is higher on the body side because the flow is more expanded in the inner region than at the body surface. A sharp drop in pressure can be observed at $y \simeq 3.3$ m because of the resultant shock formed between the inner and outer flows. The pressure in the outer flow is lower than the pressure in the inner flow. Section 2′ demonstrates that because of the curvature of the cowl outer surface, expansion occurs after the cowl bow shock; hence the pressure decreases between the bow shock and the cowl surface. This is confirmed by observing that the pressure jump (and shock strength) across the outer cowl shock is less in section 3 than section 2′. It can be seen that the pressure mismatch between the inner and outer flow is not severe. In any event, no shock enters the propulsive stream tube from the cowl trailing edge. Section 4, at the exit plane, demonstrates that the flow near the body is not as expanded as the flow near the cowl. In either case, the pressure at the exit plane is greater than the freestream pressure. Hence, the inner flow is underexpanded. Generally, further expansion would increase the

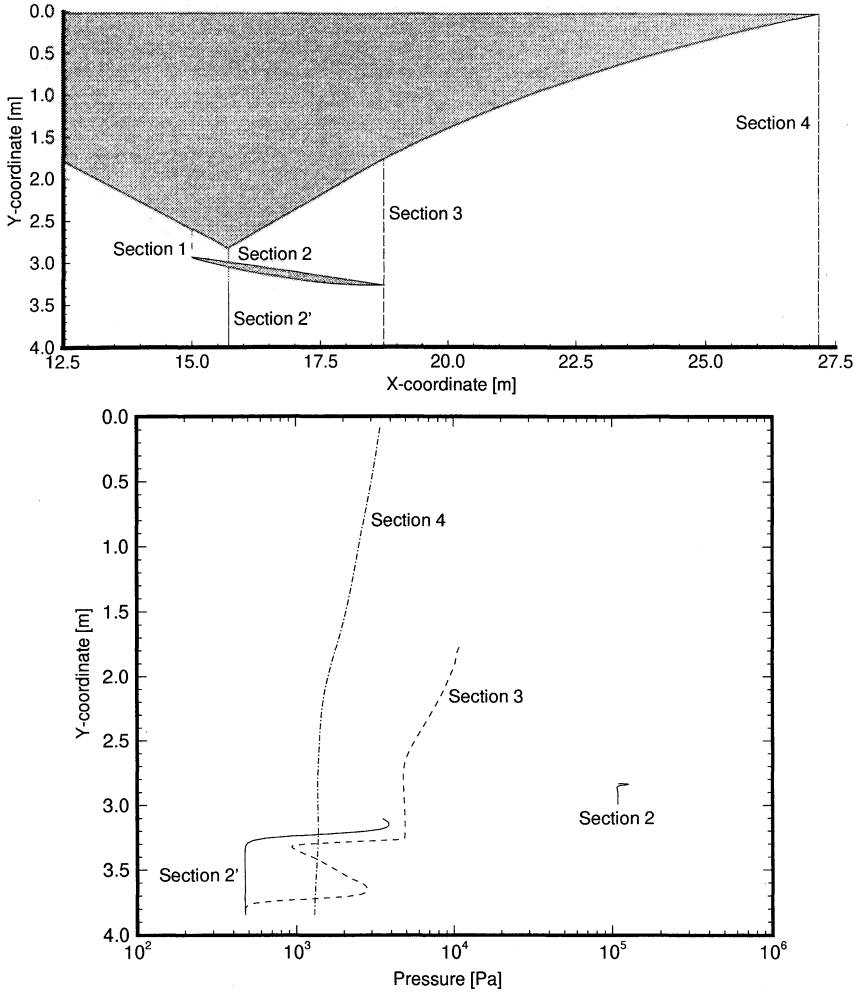

Fig. 7 Pressure along three vertical extraction lines in a Mach 14, planar shcramjet at a flight dynamic pressure of 1400 psf.

amount of thrust; however, the amount of expansion has been limited by geometrical considerations. One of the design criteria was that the flow would not be expanded above the axis, as there would be a commensurate thrust penalty by virtue of the creation of a shock on the upper surface. Figure 8 demonstrates the H_2O mass fraction and entropy production in the combustor outflow, section 2. Clearly, there is increased production of H_2O (heat release) and the entropy production is less near the cowl surface, corresponding to the shock-induced combustion region that is apparently more efficient than the detonation wave. The entropy is not seen to rise significantly between sections 3 and 4 in the propulsive stream tube; hence, it can be concluded that the flow in the nozzle is not strongly in chemical nonequilibrium. The entropy production drops off steeply in section 4 near $y \simeq 3.8$ m as the contact surface between the propulsive stream tube and outer flow is reached. Figure 9 depicts the H_2O mass fraction variations along three streamlines, starting at the inflow (Fig. 3). Streamline A passes near the centerbody, streamline C passes near the cowl surface, and streamline B is situated approximately halfway in between. After the sudden creation of H_2O and attendant heat release by the detonation wave, for each streamline the H_2O mass fraction is seen to increase substantially after exiting the combustor. The H_2O mass fraction is slightly higher along streamline C, which passes through the shock-induced combustion region. For comparison, the maximum mass fraction of H_2O, obtained for complete combustion, i.e., $H_2 + \frac{1}{2}(O_2 + 3.76\ N_2) \rightarrow H_2O + \frac{1}{2}(3.76\ N_2)$, would be 0.255. The creation of H_2O in the nozzle may be linked to the fact that the temperature is decreasing and, hence, dissociated H_2O is recombining. The bulk of recombination of H_2O occurs within the first 4 m of the nozzle, for $x \leq 19$ m. After this point the H_2O mass fraction rises only minimally.

Figure 10 shows the temperature distributions along streamlines A, B, and C. Streamline C is seen to undergo compression by both the inlet shocks and is the first to experience the sudden temperature increase by the shock-induced combustion. The temperature along streamlines B and C remain at the post-detonation value for a short distance before the streamlines undergo expansion by the centered fan (at point E, Fig. 3). Unlike streamlines B and C, streamline A, after the detonation wave, almost immediately passes through the strong expansion wave, hence the temperature is reduced rapidly. It can be observed that along streamline A, the temperature increases slightly after the detonation wave. The reason for this increase is linked to the production (recombination) of H_2O in the nozzle.

The effect of H_2O recombination in the nozzle section may be also observed in a comparison of the temperature distribution along the nozzle walls predicted by the frozen method of characteristics (MOC) and the nonequilibrium Euler solution, shown in Fig. 11. It is apparent that the temperature distribution is seen to digress significantly from the frozen flow, MOC solution. The MOC solution predicts a large, discontinuous drop in temperature at the corner of the expansion fan, and steady decrease thereafter, whereas the solution of the Euler equations reveals that the temperature increases due to recombination. The recombination of H_2O in the nozzle is hence self-limiting: H_2O is created owing to recombination reactions in the nozzle, which occur because the temperature is lower and the equilibrium shifts toward the reactants, yet, the heat released by recombination increases the temperature in the

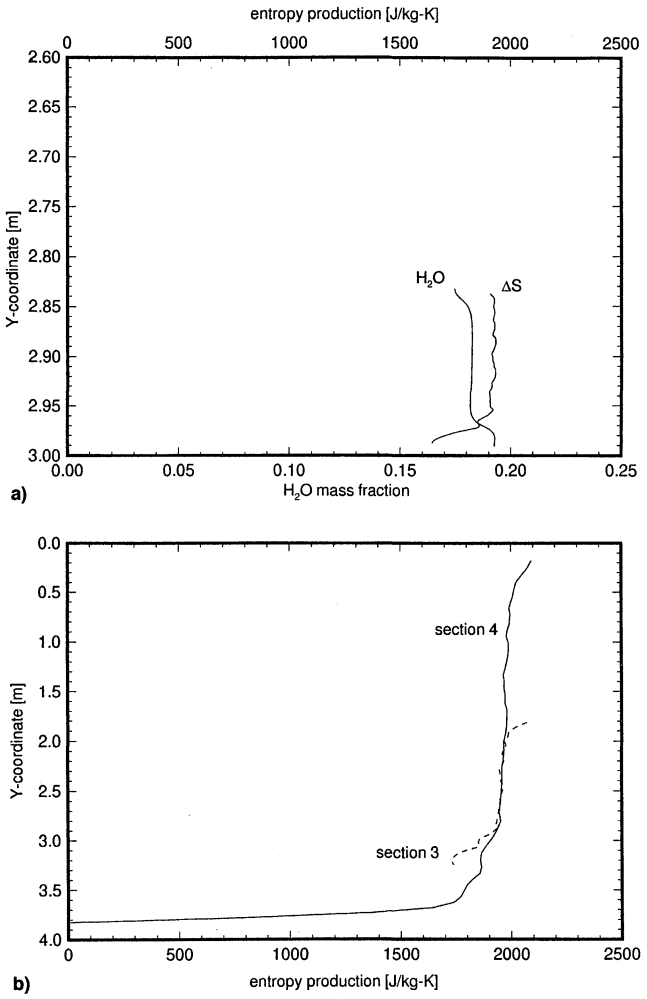

Fig. 8 Entropy and H_2O mass fraction along vertical extraction lines in a Mach 14, planar external compression shcramjet at a flight dynamic pressure of 1400 psf: a) Entropy and H_2O mass fraction at combustor outflow, section 2, and b) entropy production at sections 3 and 4.

nozzle and shifts the equilibrium point back to the products. Based on the comparison with the frozen MOC solution, H_2O recombination is seen to significantly affect the temperature in the nozzle, yet only marginally affect the pressure. This phenomenon has also been observed by Sangiovanni et al.[43]

Shcramjet Performance Characteristics

The performance of the shcramjet will be assessed in the context of various parameters and efficiencies for a constant flight dynamic pressure trajectory of q = 1400 psf (67,032 Pa), and for a stoichiometric mixture of H_2 and air.

The most prevalent measure of performance for a propulsion system is I_{sp}, which is defined here as the ratio of the net thrust to the fuel weight flow rate. Figure 12 contains the net I_{sp} for planar shcramjet configurations. The values are greater for the mixed compression shcramjet. On average, an increase of approximately 22–23% can be observed over the entire flight Mach number range. A major consequence of this figure is that the shcramjet I_{sp} is comparable to the rocket-engine specific fuel consumption at flight Mach numbers of ≃20–22. Also depicted in this figure is the fuel specific impulse for a generic scramjet calculated using the hypersonic air-breathing propulsion (HAP) computer program devised by Pratt and Heiser,[44] based on average or most-probable values of shcramjet component efficiency estimates for the same flight dynamic pressure trajectory, and the scramjet performance estimate taken from Billig[45] at q = 1000 psf in which viscous losses and

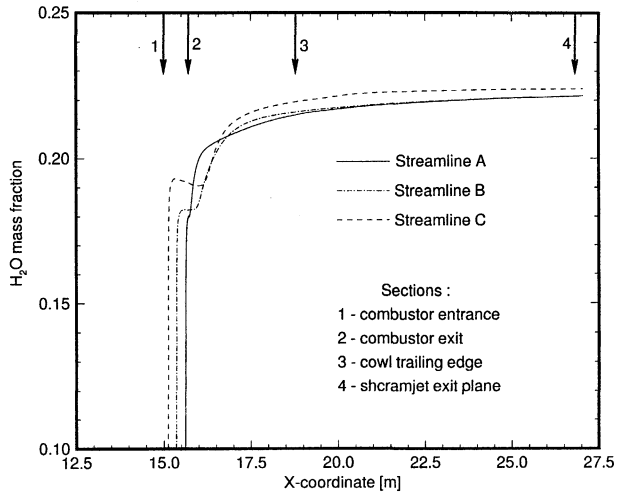

Fig. 9 H_2O mass fraction variation along three streamlines in combustor and nozzle sections for Mach 14, planar shcramjet at a flight dynamic pressure of 1400 psf.

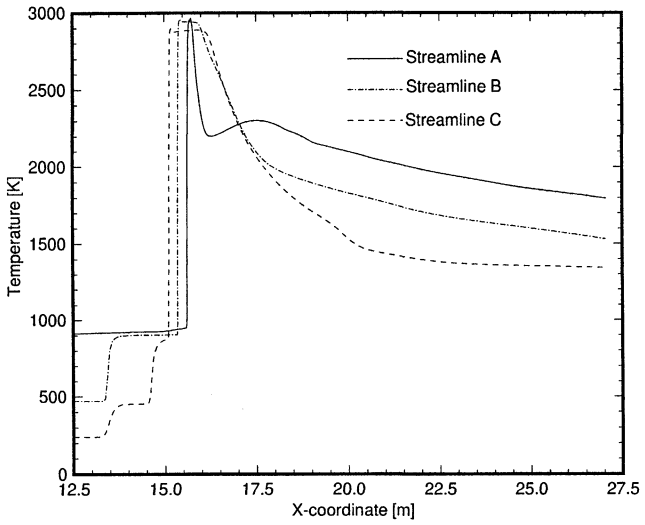

Fig. 10 Temperature (K) variation along three streamlines in combustor and nozzle section for Mach 14, planar shcramjet at a flight dynamic pressure of 1400 psf.

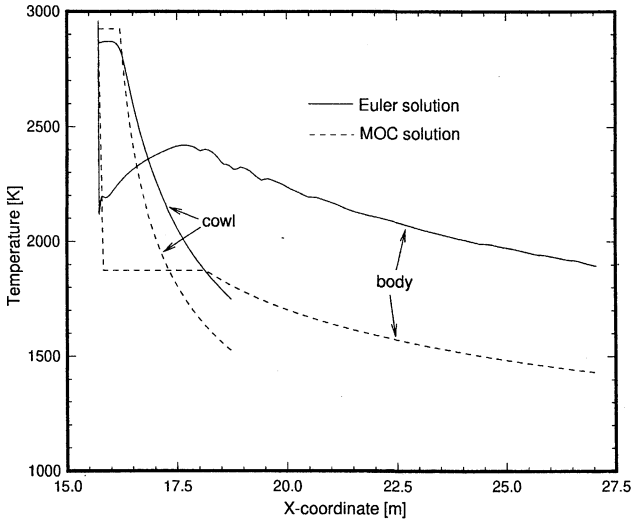

Fig. 11 Comparison of the frozen method of characteristics and full Euler solutions for temperature distribution along body and cowl nozzle surface for Mach 14, planar shcramjet at a flight dynamic pressure of 1400 psf.

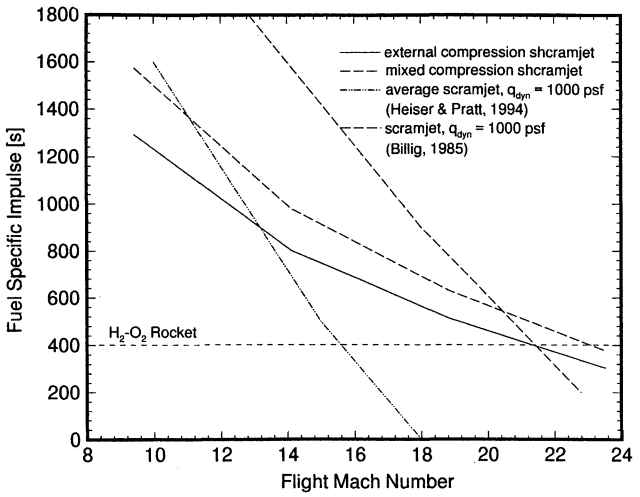

Fig. 12 Mixed vs external compression shcramjet fuel specific impulse comparison, at a flight dynamic pressure of 1400 psf; equivalence ratio ϕ = 1.

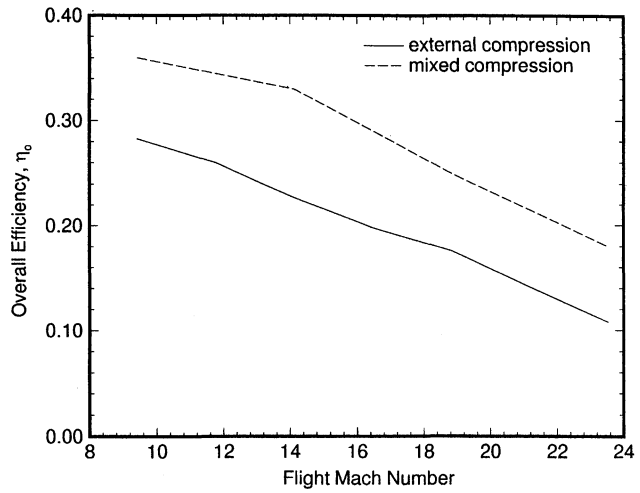

Fig. 13 Overall efficiency, η_o, for planar configuration shcramjets (external and mixed-compression) at a flight dynamic pressure of 1400 psf.

nozzle flow nonequilibrium chemistry were taken into account. The performances of the two engine concepts seem to be comparable, with the shcramjet having an advantage over the scramjet in the very high flight Mach number range. Similar trends were also observed in previous research.[16] The present, albeit first look, results show that the shcramjet can be a viable means of hypersonic propulsion; however, much additional work is required to definitely substantiate this claim.

The overall efficiency of the planar shcramjet, which is the product of thermal and propulsive efficiencies, is shown in Fig. 13. Because the propulsive efficiency is very close to unity, especially at very high flight Mach numbers, the depicted trend of the overall efficiency is virtually identical to the thermal efficiency. Clearly, the mixed compression ramjet exhibits a higher overall efficiency over the entire flight Mach number range. Figure 14 depicts the percentage contribution to the overall thrust of each shcramjet component throughout the Mach 8–24 range. A trend is observed for external compression shcramjets, whereby the thrust contribution by the cowl components (outer cowl surface, cowl combustor, and cowl nozzle) diminish as the flight Mach number increases. At Mach 24, the cowl contribution is seen to be minimized. This trend corresponds to the fact that the 3-deg overdriven Chapman–Jouguet condition reduces the cowl combustor angle to be parallel to the freestream flow at high-flight Mach numbers. For mixed-compression shcramjets this same condition produces negative thrust (drag) by the combustor wall of the cowl. As expected, the inlet and combustor drag along the body is lower than the mixed compression configuration. The body nozzle contribution to overall thrust increases as the flight Mach number increases for both configurations.

Figure 15 shows the ignition delay distances along the cowl surface in the combustor section and the total length (CF or DF, see Fig. 3) of the combustor over the considered flight Mach number range. The combustor length is governed by a number of factors including the design specification of the cowl angle and the 900 K temperature limit at the end of the compression process, which in combination dictate the ignition delay distance, the detonation wave angle and, hence, the relative geometry of the cowl and body in the combustor. The combustor length is then obtained from the intersection of the detonation and the body surface. It is evident that to satisfy the condition that the detonation wave operate at a 3-deg overdriven Chapman–Jouguet condition, the ignition delay dis-

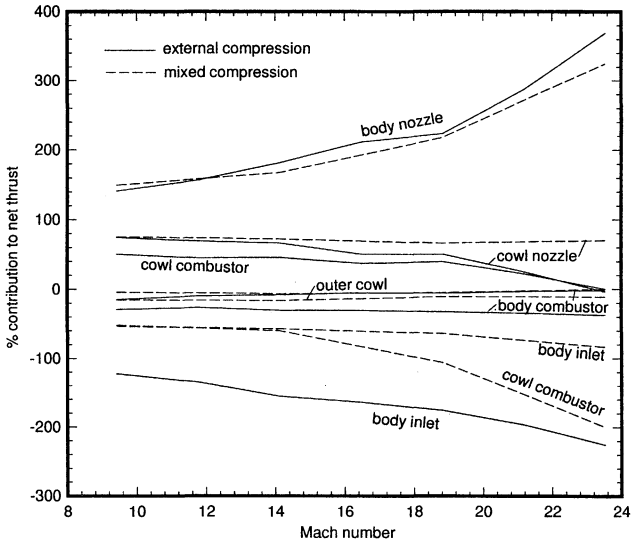

Fig. 14 Component contribution to overall thrust for planar configuration shcramjets (external and mixed-compression) at a flight dynamic pressure of 1400 psf.

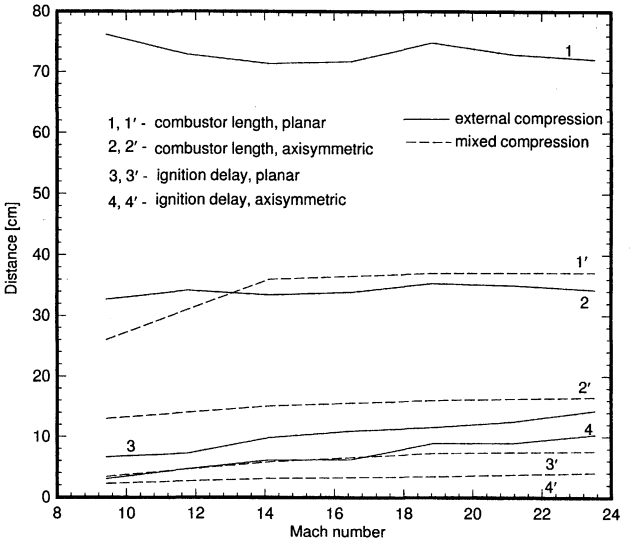

Fig. 15 Ignition delay distance in the combustor and total length of combustor for planar and axisymmetric configuration shcramjets (external and mixed-compression) at a flight dynamic pressure of 1400 psf.

tance increases substantially as flight Mach number increases. Remarkably, for planar and axisymmetric shcramjets, the combustor length remains relatively unchanged for very high flight Mach numbers. This property is of interest because an accelerating, variable-geometry shcramjet would not have to alter combustor length, but only the cowl angle. The combustor length is lower for the axisymmetric configuration by virtue of the fact that the combustor inflow area is narrower than for planar shcramjets. It can also be seen that ignition delay distances and combustor lengths are shorter for mixed compression shcramjets. Results also show that planar shcramjets exhibit marginally better performance throughout the entire range of flight Mach numbers. For more details on flowfield and performance characteristics, see Dudebout.[46]

Concluding Remarks

Results obtained in the present investigation show that a detonation wave can be used as a viable means of hypersonic propulsion. Fuel injection and mixing losses, as well as viscous losses, might be compensated for by shcramjet geometries with better performance and expansion in a three-dimensional nozzle (instead of the two-dimensional nozzle considered here). The shcramjet geometry chosen for this study is by no means optimum and it is not unreasonable to assume that performance characteristics can still be improved. Design methodologies not considered here may prove to be better suited for this mode of propulsion.

From the configurations studied here the performance of mixed compression inlet shcramjet is superior to the external compression shcramjet. It can also be surmised that shock-induced combustion is more efficient than the detonation wave (less entropy production, more heat released); hence a shcramjet model employing solely shock-induced combustion may be worth considering. With the considered design procedure, planar configuration shcramjets have slightly better performance than axisymmetric shcramjets throughout the flight envelope.

The presented methodology of investigating shcramjet performance characteristics is now being used to determine its off-design performance, i.e., the propulsive characteristics of the vehicle for flight Mach numbers other than for which it was designed to operate. The present approach is also being applied to the investigation of the effect of nonuniform fuel/air mixing, by modulating the equivalence ratio in the propulsive stream tube, on the performance characteristics of the shcramjet. A preliminary analysis of viscous and heat conduction effects, via a laminar Navier–Stokes simulation of the shcramjet flowfield, shows detonation wave–boundary-layer interaction to be a major concern. One other major concern of shcramjet flowfields, the fuel/air mixing process without premature ignition, in the propulsive stream tube ahead of the shock-induced combustion region is being addressed by considering a wall injection of hydrogen surrounded by a cool inert jet of gaseous nitrogen in a hypersonic airstream (similar to the configuration proposed by Ostrander et al.[16]) and numerically simulating the turbulent reacting flowfield. Finally, of particular importance is the basic issue of the stability of steady detonation waves in the combustor. Undoubtedly, research in shock-induced combustion ramjets is at an early stage and much more work is needed to ascertain the feasibility of shcramjets.

References

[1]Murthy, S. N. B., and Curran, E. T., *High-Speed Flight Propulsion Systems*, Vol. 137, Progress in Astronautics and Aeronautics, AIAA, Washington, DC, 1991.

[2]Bushnell, D. M., "Hypervelocity Scramjet Mixing Enhancements," *Journal of Propulsion and Power*, Vol. 11, No. 5, 1995, pp. 1088–1090.

[3]Bogdanoff, D. W., "Advanced Injection and Mixing Techniques for Scramjet Combustors," *Journal of Propulsion and Power*, Vol. 10, No. 3, 1994, pp. 183–190.

[4]Sislian, J. P., and Atamanchuk, T. M., "Aerodynamic and Propulsive Performance of Hypersonic Detonation Wave Ramjets," *Proceedings of the 9th International Symposium on Air Breathing Engines*, AIAA, Washington, DC, 1989, pp. 1026–1035.

[5]Roy, M. M., "Moteur Thermiques," *Comptes Rendus de l'Academie des Sciences*, Vol. 222, No. 1, 1946.

[6]Dunlap, R., Brehm, R. L., and Nicholls, J. A., "A Preliminary Study of the Application of Steady-State Detonation Combustion to a Reaction Engine," *Journal of Jet Propulsion*, Vol. 28, No. 6, 1958, pp. 451–456.

[7]Sargeant, W. H., and Gross, R. A., "A Detonation Wave Hypersonic Ramjet," TN 589, U.S. Air Force Office of Scientific Research, Fairchild Engine and Airplane Corp., New York, 1959.

[8]Townend, L. H., "Detonation Ramjets for Hypersonic Aircraft," Royal Aircraft Establishment, TR 70218, Nov. 1970.

[9]Morrison, R. B., "Evaluation of the Oblique Detonation Wave Ramjet," NASA, CR 145358, Jan. 1978.

[10]Morrison, R. B., "Oblique Detonation Wave Ramjet," NASA, CR 159192, Jan. 1980.

[11]Billig, F. S., "External Burning in Supersonic Streams," *Proceedings of the 18th International Astronautical Congress*, Vol. 3, 1968, pp. 23–54.

[12]Billig, F. S., "Combustion Processes in Supersonic Flow," *Proceedings of the 7th International Symposium on Air Breathing Engines*, AIAA, Washington, DC, 1985, pp. 245–256.

[13]Chernyi, G. G., "Supersonic Flow Past Bodies with Formation of Detonation and Combustion Fronts," *Problems of Hydrodynamics and Continuum Mechanics*, 1969, pp. 145–169 (English edition).

[14]Chushkin, P. I., "Combustion in Supersonic Flows Past Various Bodies," *Journal of Computational Mathematics and Mathematical Physics*, Vol. 1, No. 6, 1969, pp. 1367–1377.

[15]O'Brien, C. J., and Kobayashi, A. C., "Advanced Earth-to-Orbit Propulsion Concepts," AIAA Paper 86-1386, June 1986.

[16]Ostrander, M. J., Hyde, J. C., Young, M. F., and Kissinger, R. D., "Standing Oblique Detonation Wave Engine Performance," AIAA Paper 87-2002, June 1987.

[17]Ashford, S. A., and Emanuel, G., "Oblique Detonation Wave Engine Performance Prediction," *Journal of Propulsion and Power*, Vol. 12, No. 2, 1996, pp. 322–327.

[18]Sheng, Y., and Sislian, J. P., "A Model of a Hypersonic Two-Dimensional Oblique Detonation Wave Ramjet," TN 257, Univ. of Toronto Inst. for Aerospace Studies, ON, Canada, July 1985.

[19]Atamanchuk, T. M., and Sislian, J. P., "Performance Characteristics of Hypersonic Detonation Wave Ramjets." *Proceedings of the 75th AGARD Symposium on Air-Breathing Engines*, 1990, pp. 25-1–25-13.

[20]Atamanchuk, T. M., and Sislian, J. P., "On-and-Off Design Performance Analysis of Hypersonic Detonation Wave Ramjets," AIAA Paper 90-2473, July 1990.

[21]Atamanchuk, T. M., Sislian, J. P., and Dudebout, R., "An Aerospace Plane as a Detonation Wave Ramjet/Airframe Intgrated Waverider," AIAA Paper 92-5022, Dec. 1992.

[22]Sislian, J. P., and Dudebout, R., "Hypersonic Shock-Induced Combustion Ramjet Performance Analysis," *Proceedings of the 11th International Symposium on Air Breathing Engines*, AIAA, Washington, DC, 1993, pp. 413–420.

[23]Dudebout, R., and Sislian, J. P., "Numerical Simulation of Hypersonic Shock-Induced Combustion Ramjet Flowfields," AIAA Paper 94-3098, June 1994.

[24]Sislian, J. P., Dudebout, R., Schumacher, J., Islam, M., and Oppitz, R., "Inviscid Propulsive Characteristics of Hypersonic Scramjets," AIAA Paper 96-4535, Nov. 1996.

[25]Sislian, J. P., Dudebout, R., and Oppitz, R., "Inviscid On-Design Propulsive Characteristics of Hypersonic Shock-Induced Combustion Ramjets," TR 352, Univ. of Toronto Inst. for Aerospace Studies, ON, Canada, Feb. 1997.

[26]Menees, G. P., Adelman, H. G., Cambier, J-L., and Bowles, J. V., "Wave Combustors for Trans-Atmospheric Vehicles," 9th International Symposium on Air Breathing Engines, AIAA, Washington, DC, 1989.

[27]Nusca, M. J., and Kruczynski, D. L., "Reacting Flow Simulation for a Large-Scale Ram Accelerator," *Journal of Propulsion and Power*, Vol. 12, No. 1, 1996, pp. 61–69.

[28]Li, C., Kailasanath, K., and Oran, E. S., "Stability of Projectiles in Thermally Choked Ram Accelerators," *Journal of Propulsion and Power*, Vol. 12, No. 4, 1996, pp. 807–809.

[29]Yungster, S., and Bruckner, A. P., "Computational Studies of Superdetonative Ram Accelerator Models," *Journal of Propulsion and Power*, Vol. 8, No. 2, 1992, pp. 457–463.

[30]Yungster, S., and Rabinowitz, M. J., "Computations on Shock-Induced Combustion Using a Detailed Methane-Air Mechanism," *Journal of Propulsion and Power*, Vol. 10, No. 5, 1994, pp. 609–617.
[31]Yungster, S., "Numerical Study of Shock-Wave/Boundary-Layer Interactions in Premixed Combustible Gases," *AIAA Journal*, Vol. 30, No. 10, 1992, pp. 2379–2387.
[32]Jachimowsky, C. J., "An Analytical Study of the Hydrogen-Air Reaction Mechanism with Application to Scramjet Combustion," NASA TP-2791, Dec. 1988.
[33]Yoon, S., and Jameson, A., "An LU-SSOR Scheme for the Euler and Navier-Stokes Equations," AIAA Paper 87-600, Jan. 1987.
[34]Yoon, S., and Jameson, A., "A Lower-Upper Symmetric Gauss-Seidel Method for the Euler and Navier-Stokes Equations," *AIAA Journal*, Vol. 26, No. 9, 1988, pp. 1025, 1026.
[35]Yee, H. C., "Upwind and Symmetric Shock-Capturing Schemes," NASA TM-89464, Feb. 1987.
[36]Lehr, H. F., "Experiments on Shock-Induced Combustion," *Astronautica Acta.*, Vol. 17, Oct. 1972, pp. 589–597.
[37]Dudebout, R., and Sislian, J., "Resolution of Exothermic Blunt Body Flows," *Proceedings of the 3rd Conference of CFD Society of Canada*, Banff, AL, Canada, 1995, pp. 401–408.
[38]Drabczuk, R., Rolader, G. E., Sinha, R., and Clothiaux, E., "Fundamental Research to Advance Ram Accelerator Technology," *U.S. Air Force Contractor's Meeting* (Atlantic City, NJ), 1993, pp. 65–68.
[39]Hammer, S. S., and Agosta, V. D., "Scramjet Nozzle Analysis," Propulsion Sciences, Int. Rept. 70-1, Feb. 1970.
[40]Migdal, D., "Supersonic Annular Nozzles," *Journal of Spacecraft and Rockets*, Vol. 9, No. 1, 1972, pp. 3–6.
[41]Vander Veen, R., Gentry, R., and Hoffman, J. D., "Design of Shrouded-Plug Nozzles for Maximum Thrust," *AIAA Journal*, Vol. 12, No. 9, 1974, pp. 1193–1198.
[42]Park, H.-K., "Model of an Aero-Space Plane Based on an Idealized Cone-Derived Waverider Forebody," Ph.D. Dissertation, Univ. of Oklahoma, Norman, OK, 1990.
[43]Sangiovanni, J. J., Barber, T. J., and Syed, S. A., "Role of Hydrogen/Air Chemistry in Nozzle Performance for Hypersonic Propulsion System," *Journal of Propulsion and Power*, Vol. 9, No. 1, 1993, pp. 134–138.
[44]Pratt, D. T., and Heiser, W. H., *Hypersonic Airbreathing Propulsion*, AIAA Education Series, Washington, DC, 1994.
[45]Billig, F. S., "Proposed Supplement to Propulsion System Management Support Plan," Defense Advanced Research Project Agency, Oct. 1985.
[46]Dudebout, R., "Numerical Simulation of Hypersonic Shock-Induced Combustion Ramjet Flowfields," Ph.D. Dissertation, Univ. of Toronto, ON, Canada, 1996.